International Journal of Technology 14(1) 129-141 (2023)
Received September 2021 / Revised September 2021 / Accepted October 2022

International Journal of Technology

Clay and Zeolite-Clay Based Monoliths as Adsorbents for the Hg(II) Removal from the Aqueous Solutions

Darmadi[1*], Mirna Rahmah Lubis[1], Munadiya Masrura[2], Aziz Syahfatra[2], Mahidin[1]

[1]*Chemical Engineering Department, Universitas Syiah Kuala, 23111, Banda Aceh, Indonesia*
[2]*Processing Technology Laboratory, Universitas Syiah Kuala, 23111, Banda Aceh, Indonesia*

Abstract. Clay and zeolite-clay-based monoliths (ZCBM and CBM) were used as mercury removal adsorbents in aqueous solutions. Clay and zeolite-clay-based monoliths (40 holes in 18 mm diameter) were obtained by extruding the material with water. This research aimed to investigate and compare the capacities and kinetics of two adsorbents, zeolite-clay, and clay-based monoliths, to identify the most effective adsorbent in adsorbing mercury(II) ions. The ZCBM and CBM crystal structures were characterized using a scanning electron microscope, Brunauer–Emmett–Teller (BET) theory, and an X-ray diffractometer. The effect of contact time (40, 80, 120, 160, 200, and 240 minutes), adsorbent doses (1 and 2 mg/L), as well as initial concentrations (1–5 mg/L) were variables evaluated. The most effective adsorbent is identified by selecting the highest adsorption efficiency. These equilibrium experimental data and the adsorption kinetics were investigated in a batch-type reactor. Data of equilibrium were examined with the Freundlich, Langmuir, and BET isotherm models by observing the lowest sum of squares (SSE) value. This Langmuir isotherm model indicated the most significant fit to the adsorption data of both adsorbents. To examine the kinetic data, the pseudo-first-order and pseudo-second-order adsorption kinetic models were implemented. This adsorption kinetic characterization using both ZCBM and CBM was well displayed by the pseudo-first-order model. Even though the maximum equilibrium adsorption capacity was 0.167 mg/g for ZCBM, but SSE value showed that CBM was the adsorbent with the highest adsorption efficiency, namely 72.3%. Therefore, CBM becomes the most effective adsorbent for mercury removal from water.

Keywords: Adsorption; Clay; Isotherm; Mercury; Monolith

1. Introduction

Mercury and its components pose a significant threat to living creatures and the environment when they are present in industrial wastewater and enter water systems. They can be absorbed by the skin, gastrointestinal tract, and lungs, as well as circulates in the blood, which can cause several health problems, such as dysfunction of the nerves, and even death (Nabais *et al.*, 2006). Recently, researchers have thoroughly studied the remediation and removal of heavy metals, with several extensively used techniques, such as biological treatment, adsorption, etc. Adsorption is one of the separation methods in which particular components of a solution are moved to the side of a solid adsorbent (Sudibandriyo and Putri, 2020). Considering mercury's low solubility, adsorption is the most appropriate method for its removal due to its large absorp-

*Corresponding author's email: darmadi@unsyiah.ac.id, Tel.: (0651) 7552222; Fax: (0651) 7552222
doi: 10.14716/ijtech.v14i1.5134

absorption capacity.

Adsorbents are modified to boost their adsorption capacity. The modification includes cross-linking, grafting, and physical mixing with large surface area materials (Bahrudin *et al.*, 2020) or monolith structures to obtain better properties. Various adsorbents, including chitosan composite, modified lignin, kaolin clay, natural zeolite, and activated carbon, have been demonstrated to effectively eliminate mercury from the water. Chitosan composite has been utilized for metal removal (Jawad, Mubarak, and Abdulhameed, 2019a), dye removal, and pharmaceuticals (Malek *et al.*, 2020). Several materials, such as fly ash, zinc oxide, and montmorillonite (clay) are used for the preparation of chitosan composites with improved adsorptive and physiochemical characteristics (Mohammed *et al.*, 2020).

The chitosan-zeolite composite is mentioned in the section on pollutant removals, such as the removal of Fe, Cr, and Ni ions, as well as adsorptions of methyl orange and humic acid (Jawad *et al.*, 2020a). Despite chitosan composite was widely utilized in many applications like wastewater treatment (Jawad, Mubarak, and Abdulhameed, 2019b), adsorption with zeolites is considered a favorable method (Basuki *et al.*, 2021). Studies indicate that chitosan composite can improve surface properties (Jawad, Abdulhameed, and Mastuli, 2020b), but activated carbon and natural zeolites have the highest efficiency among these adsorbent types. Zeolite is a naturally occurring crystalline alumina silicate compound that can also be synthesized commercially. It has been widely used as a catalyst or adsorbent because of its thermal stability and non-flammability (Karamah *et al.*, 2019). Natural zeolites, such as clinoptilolite, can contain more than 50 different minerals, including various cations, such as K^+, Na^+, Mg^{2+}, or Ca^{2+}. Synthetic zeolites usually contain only a single cation of K^+ or Na^+, so they have a relatively uniform pore size and diameter. Natural clinoptilolite modified with gold successfully raised its removal efficiency of Hg(II) to 44% higher than natural clinoptilolite including at a very low amount of adsorbent (Attari, 2015). In addition to activated carbon, clay is an effective adsorbent for removing mercury from the water. Clay is a common mineral on earth with smooth silicate grains. Clay has a large surface area, approximately 800 m^2/g, which causes a high adsorption capacity (Kausar *et al.*, 2018) to remove heavy metals from wastewater.

A previous study investigated mercury (II) removal with natural and iron-modified clinoptilolite in an incubator shaker (Ugrina *et al.*, 2020). However, no particular monolithic structure has been suggested yet. Monoliths contain solid parallel holes or channels filled by thin partitions in a honeycomb structure. The channels may be circular, hexagonal, triangular, or rectangular (Govender and Friedrich, 2017). Most ceramic monoliths are made using extrusion molding, which is a frequently used process to make highly porous materials for adsorption. The advantages of a honeycomb monolith as an adsorbent include its simple scale-low-pressure drops, efficient mass transfer interface, and adequate mechanical and thermal properties (Ahrouch *et al.*, 2019a). Therefore, the focus of this research was to examine and compare the use of a zeolite/clay mixture (2:1) and 100% clay in a honeycomb-monolith structure to remove mercury(II) ions from an aqueous solution. The ratio was selected after trying to mix the zeolite and clay to obtain a sticky paste. If only zeolite was utilized thus the dough would be fragile.

2. Methods

2.1. Materials

Zeolite and clay were utilized as raw materials in this study. They are prepared to ensure uniform sizes using a ball mill and sieving with a 100-mesh sieve. For ZCBM, zeolite and clay powder were combined in a 2:1 ratio to produce a homogenous paste, which was

then molded using a 304 molder. Clay was added to the honeycomb monolith structure as a binding agent (the dimensions of the monolith are 18 mm in diameter, 20 mm in height, and 40 holes with a pitch of 2 mm). The extruded honeycomb structure contained straight channels to offer a low-pressure drop. For CBM, only clay was processed into a homogenous paste and then molded. The molded paste changed into monoliths after being dried at room temperature for two days; then they were calcinated in a muffle furnace (Furnace 51148, Nabertherm Germany) at 600°C for three hours (Figure 1). Figure 1 presents a schematic diagram of the adsorbent preparation from ZCBM and CBM.

Figure 1 Schematic diagram of the adsorbent preparation

2.2. Characterization of the ZCBM and the CBM

The crystalline structure and chemical composition of the zeolite and clay was analyzed using an X-ray diffractometer (X'Pert3 Powder & Empyrean, PANalytical). A scanning electron microscope (FEI, Inspect-S50) was utilized to examine the surface morphology of the ZCBM and CBM. Characterization of ZCBM and CBM was carried out with N_2 physisorption at -196ºC with Micromeritics ASAP 2020. The obtained isotherms were utilized to estimate the BET-specific surface area and the micro and meso-porosities.

2.3. Adsorption

The mercury (II) ion was adsorbed by ZCBM and CBM using the batch equilibration method in a batch reactor (Erlenmeyer 250 mL) containing a 200-mL mercury solution. The solution was adsorbed at room temperature for 240 minutes with various initial concentrations of mercury (i.e., 1, 2, 3, 4, and 5 mg/L) to examine the adsorption capacity. It was stirred continuously using a Kotterman shaking water bath. After that, each Hg solution was taken 2 mL and analyzed at a wavelength of 253.7 nm using a mercury analyzer (Nippon Instruments Corporation). The data were examined to discover efficiency, adsorption capacity, and the fittest isotherm model among Freundlich, Langmuir, and BET with non-linear method analysis by observing the lowest sum of squares (SSE) value. Both pseudo-first and pseudo-second-order kinetic equations– are applied.

3. Results and Discussion

3.1. Crystal Structure and Size Characterization

X-Ray Diffraction shows that adsorbents consist of SiO_2, Al_2O_3, and montmorillonite, as identified by some peaks according to ICDD PDF No. 01-0649, ICDD PDF No. 42-1468, and Physics and Chemistry of Minerals 35 (2008).

In Figure 2, the strong peaks at 20.48˚ and 26.145˚ as well as the lower peaks at 25.3˚; 37.4˚; 42.9˚; and 67.65˚ are estimated as SiO_2 (Quartz) and Al_2O_3 (aluminate), respectively. A weak peak identifies a low content of Al_2O_3 mineral so the value of the Si/Al ratio is high. A Si/Al ratio greater than four indicates that these adsorbents have a hydrophobic surface and a high thermal resistance; they are thus recommended to be implemented.

In addition, X-ray diffraction is utilized to estimate the mean size of crystals on the monolith adsorbent. Its full width at half maximum (FWHM) is analyzed with profile fitting

to estimate the mean crystallite size with the Scherrer equation. By calculating the FWHM, the sizes of zeolite and clay crystals are 11.87 and 27.25 nm, respectively. Each pore size contributes to the whole adsorption isotherm in proportion to its part of the pore volume or the total area of the adsorbent sample.

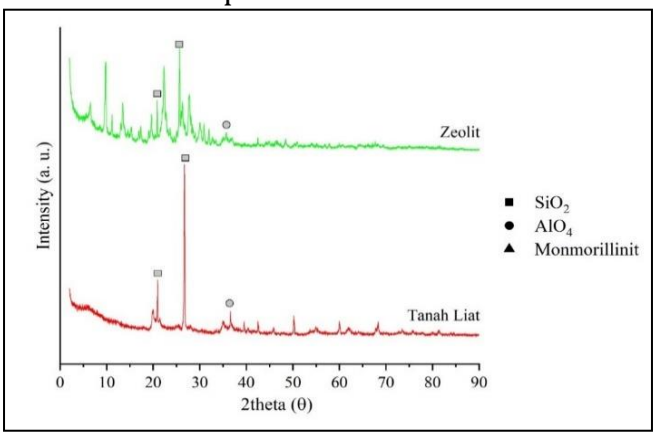

Figure 2 X-ray diffraction pattern of zeolite and clay adsorbents

3.2. Adsorbent Surface Characterization

As depicted in Figures 3a and 3b, a 7000-magnification SEM is used to observe the surface morphology of both adsorbents. Figure 3a shows that the zeolite-clay-based monolith adsorbent has irregular pores and particle shapes. The irregular pores are similar to those described in a previous study, reporting that modified zeolite monoliths have a rod and spherical-like pores by processing the zeolite powder with carbon material (Akhtar *et al.*, 2014). On the other hand, the clay-based monolith adsorbent has regular pore and particle shapes, as shown in Figure 3b. However, the particles are formed of various sizes and are not evenly distributed across the surface. Consequently, they can increase the occurrence of entrapment during the adsorption process. The apparent loss of CBM roughness in Figure 3b can be reasonably connected to the larger compaction of the CBM grains because of the extrusion. The various sizes resemble previous studies demonstrating that the clay monolith is composed of the particle agglomerate with heterogeneous size but irregular shape. Similar images were obtained for other smectite clay types (Ahrouch *et al.*, 2019b).

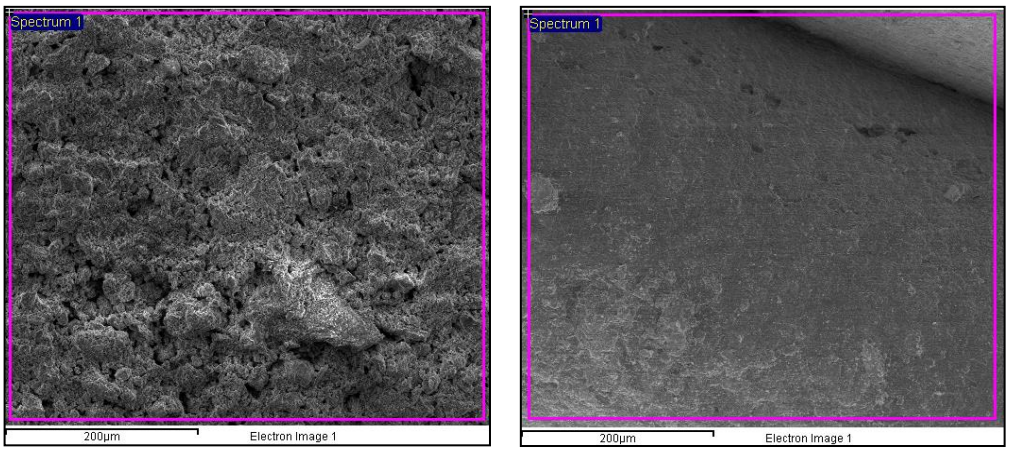

(a) (b)

Figure 3 Scanning electron microscope micrographs of (a) ZCBM and (b) CBM adsorbents

3.3. Pore Characterization

BET is the standard method for analyzing the N_2 adsorption isotherm for a sample at −197.5 °C based on the specific surface area. The N_2 adsorption-desorption isotherm was calculated with the BJH analysis to estimate the average pore size of the monolith adsorbent and the resulting curve is illustrated in Figure 4.

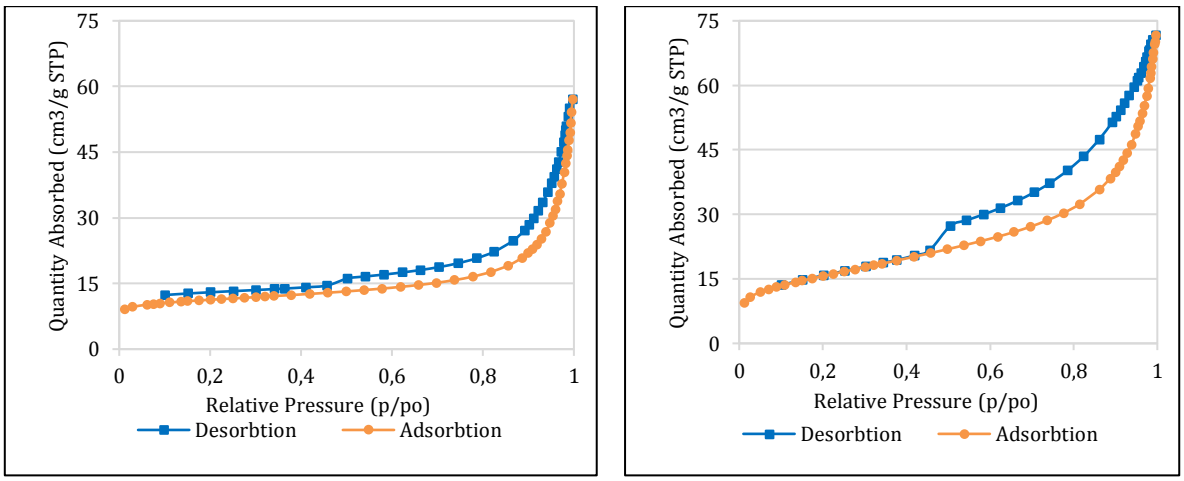

Figure 4 Nitrogen adsorption-desorption plots of (a) ZCBM and (b) CBM adsorbent

As a porous medium with mesoporous pore size, ZCBM and CBM adsorbents implied a type IV adsorption-desorption isotherm (Lapham and Lapham, 2019). This is confirmed by evidence that the mesoporous pore volumes of the ZCBM and CBM samples are dominant indicating that both adsorbents have a great ability for heavy metal adsorption. As shown in Table 1, the results of nitrogen adsorption-desorption reveal the texture of the monolith adsorbent, comprising the pore volume, the average pore diameter, and the BET surface area.

Table 1 The pore characteristics of the monolith adsorbent

Sample	BET Surface Area (m^2/g)	Average pore diameter (nm)	Pore Volume (cm^3/g)		
			Micro	Meso	Macro
ZCBM	36.396	8.790	0.211	1.800	0.178
CBM	55.065	7.812	0.300	2.013	0.157

3.4. Adsorption Capacity and Efficiency

The mercury solution concentration (Ct) curve presented in Figure 5 reveals that the adsorption rate of Hg(II) ions on ZCBM and CBM decreases with the increase of contact time (t). This indicates that the adsorption rate of mercury ions increases with time and the initial concentration. A large initial concentration allows for a larger driving force and eliminates obstacles in a mass transfer phenomenon. The process increases the absorption rate because the mercury ions in this adsorbate solution move more easily to many active sites on an adsorbent surface with good mass transfer.

As can be seen in Figure 6, the adsorption efficiency is the percentage of mercury ions adsorbed by both adsorbents. The efficiency is calculated by the following equation (Delgado *et al.*, 2019):

$$\% \text{ Efficiency} = \frac{Co\text{-}Ce}{Co} \times 100\% \quad (1)$$

The adsorption efficiency tends to rise as contact time increases. Most of the active sites on this adsorbent's surface have not yet been filled by Hg(II) ions, hence the concentration rises rapidly within the first 120 minutes.

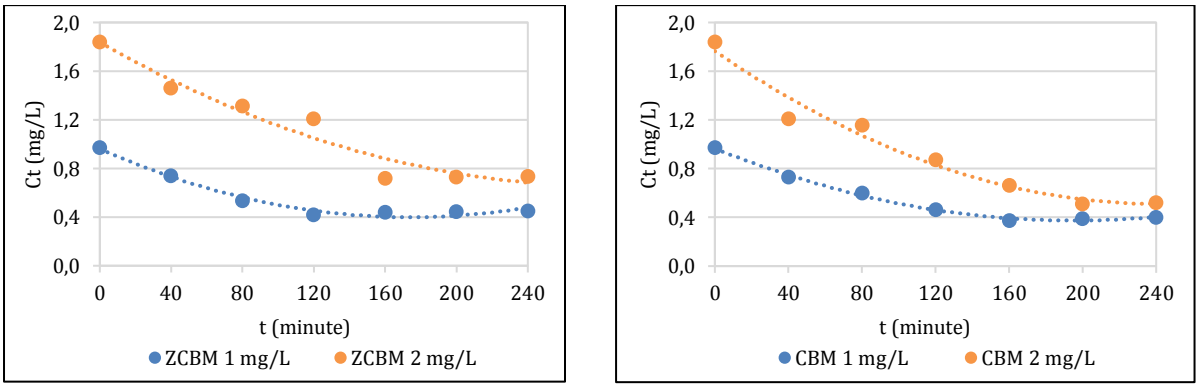

(a) (b)

Figure 5 The effect of the time on the adsorption rate for (a) ZCBM; and (b) CBM adsorbents

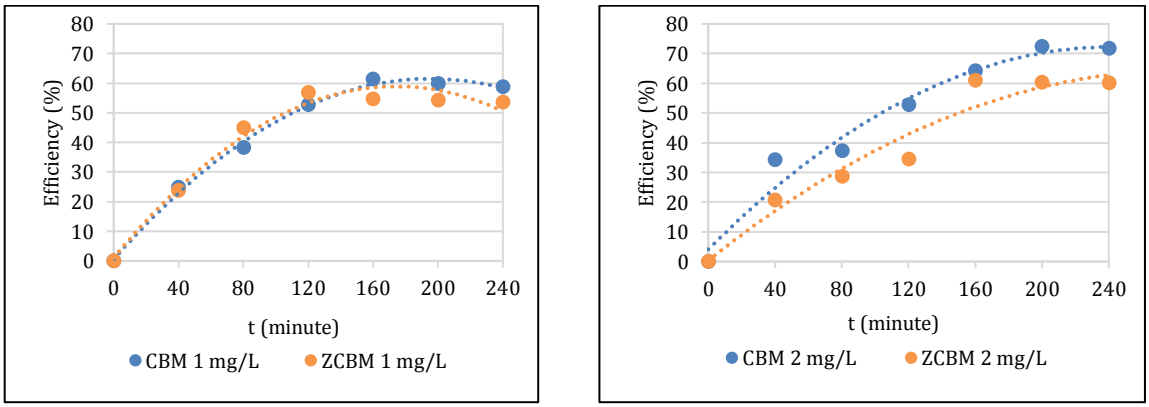

(a) (b)

Figure 6 The effect of contact time on adsorption efficiency in (a) 1 mg/L; and (b) 2 mg/L solution

The adsorbent with the highest adsorption efficiency is CBM, with an efficiency of 72.3%, followed by ZCBM, with an efficiency of 60.8% The efficiency obtained in this study is relatively high compared to the adsorbent in the form of ordinary powder of clay 63.5% (Park *et al.*, 2019) and zeolite 57% (Ugrina *et al.*, 2020). The adsorption efficiency of CBM monolith is still low because of less favored contact time for its adsorption, namely 240 minutes or twice lower than 500 minutes in a previous study (Ahrouch *et al.*, 2019).

3.5. Adsorption Isotherms

A non-linear method is used because it is more appropriate for the research of isotherm equilibrium, and advantageous because the error distribution cannot be altered as easily and quickly (Vilela *et al.*, 2019). Figure 7 depicts the nonlinear equations for the BET, while Langmuir and Freundlich models are represented by Equations 2-4 (Darmadi *et al.*, 2021).

$$q_e = \frac{q_s C_{BET} C_e}{(C_o - C_e)\left[1 + (C_{BET} - 1)\left(\frac{Ce}{Co}\right)\right]} \quad (2)$$

$$q_e = \frac{K_L \times Ce}{1 + a_L \times Ce} \quad (3)$$

$$q_e = Kf \times Ce^{1/n} \quad (4)$$

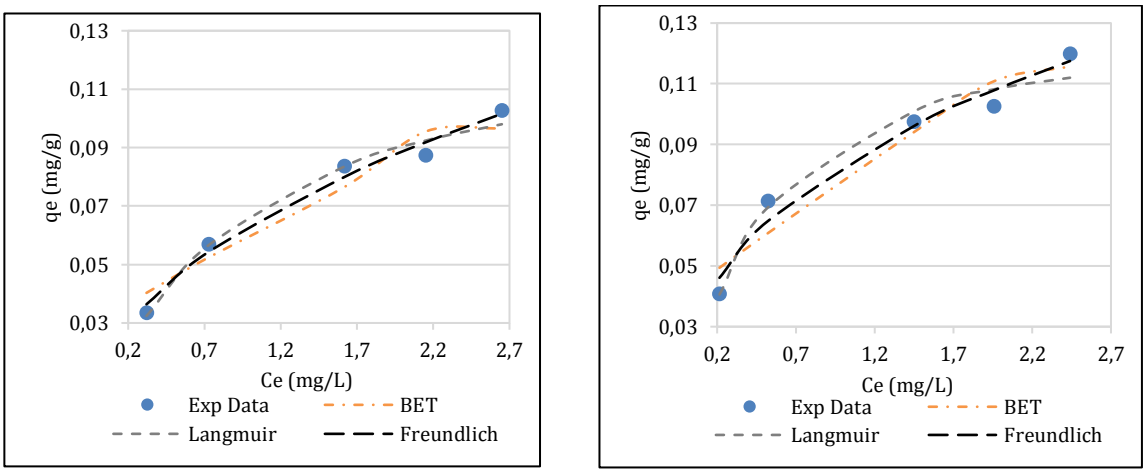

Figure 7 The congruence of data and adsorption isotherm model in (a) ZCBM and (b) CBM adsorbents

The add-in solver tool applied by Microsoft® Excel is used to estimate the isotherm parameters because the non-linear equations are harder to break than the linear equations. The tool solves the equation using the concept of the generalized reduced gradient (GRG), which is regarded as one of the most accurate non-linear programming techniques available. This SSE is implicated as the value of the minimal objective function to result in the best isotherm parameters and to minimalize the difference between theoretical and experimental data.

The greatest monolayer maximum capacity (Q0) from both Langmuir isotherm models is shown by the ZCBM adsorbent (0.137 mg/g). The highest Langmuir constants (a_L and K_L) are found in the CBM adsorbent (0.269 L/g and 1.981 L/mg, respectively).

The highest adsorbent capacity (K_f) of both Freundlich isotherm models is shown by the CBM adsorbent (0.83 mg/g). The n constant values are ordered from the highest (2.595 for CBM) to the lowest (2.061 for ZCBM). In the Freundlich isotherm, the higher the n value, the stronger the bond energy between an adsorbent and adsorbates during the adsorption phenomenon. Moreover, if n > 1, the adsorption process is favorable. Therefore, based on the Freundlich isotherm, the adsorption with both types of adsorbents was favourable.

In the BET isotherm model, the C_{BET} values from the ZCBM and CBM adsorbents are 1.419 and 5.189 L/mg, respectively. Although CBM adsorbent has the highest C_{BET} constant, the obtained value is still relatively low. C_{BET} value <10 indicates the weak interaction between this adsorbent surface and the adsorbate ions (Qiu *et al.*, 2019). The BET isotherm model is considered to be more suitable for describing gas adsorption (Lapham and Lapham, 2019).

The best isotherm model is determined by identifying the lowest SSE value among the three models. The ZCBM and CBM adsorbents fit the Langmuir isotherm model. This model indicates that adsorption occurs on the adsorbent; the active sites are limited on this adsorbent surface. This adsorption process occurs in a single layer (monolayer) on this adsorbent surface composed of homogeneous active sites, which are identical and energy-equivalent. The adsorbent can only adsorb uniformly one Hg(II) ion for each active site, and there are no binding energy interactions among adsorbed adjacent Hg(II) molecules. Table 5 displays the maximum adsorption capacities based on several adsorbents.

Table 2 Maximum adsorption capacity of several adsorbents for Hg(II)

Adsorbent	q_{max} (mg/g)	References
Bentonite monolith	0.187	Darmadi *et al.*, 2021
Chalcone-based dithiocarbamate derivative	13.5	Khor *et al.*, 2017
Chitosan-polyurethane foam	0.313	Darmadi *et al.*, 2018
Coal fly ash	0.44	Attari *et al.*, 2017
Fe-Sn-MnO_x	3.75	Xu *et al.*, 2015
Ion-imprinted polymer monoliths	0.046	Rahman *et al.*, 2017
Multifunctional Magnetic Mesoporous Silica Nanocomposite	17.7	Wang *et al.*, 2018
Phenol-glycol cross-linked polymers	2.6	Al Hamouz, 2018
Sugarcane bagasse	11.47	Giraldo *et al.*, 2019
Sulfur modified zeolites	12.1	Fang *et al.*, 2018

Several criteria based on Langmuir isotherm parameters are evaluated to determine the most effective adsorbent for Hg(II) adsorption. As previously stated, the ZCBM adsorbent showed the highest Q_o, whereas the CBM adsorbent demonstrated the highest K_L and a_L. K_L is more important than Q_o at extremely low mercury concentrations. The high adsorption affinity indicates an increase in adsorption efficiency and a stronger bond energy between the adsorbent and the adsorbate. In the Langmuir isotherm, the K_L is a parameter that reflects the adsorption affinity of a material/adsorbent. Therefore, CBM is the most effective adsorbent for Hg(II) adsorption, because of its highest K_L and a_L values, which indicate that CBM has a wide surface area. The maximum absorption capacity is proportional to the surface area. The Langmuir isotherm is then analyzed with a dimensionless constant, namely the equilibrium parameter (R_L) obtained from Equation 5:

$$R_L = \frac{1}{1 + k_L.Co} \tag{5}$$

While the R_L value is 0, $0 < R_L < 1$, $R_L = 1$, and $R_L > 1$, the adsorption is declared irreversible, good, linear, and not good, respectively. Both R_L values of ZCBM and CBM were obtained in the range of $0 < R_L < 1$, which indicates a favorable adsorption process in both adsorbents.

3.6. Adsorption Kinetics

Adsorption kinetics is the adsorption rate of adsorbate related to the residence time on the adsorbent, the data are used to obtain the optimum conditions for the adsorption. The rate of Hg(II) ion adsorption by both adsorbents is calculated utilizing Lagergen's pseudo-first and Ho's pseudo-second-order equations by non-linear as well as linear methods. A pseudo-first-order kinetic reaction is a reaction with an adsorption rate only proportional to the first power of a reactant concentration. Equations 6-7 describe linear and nonlinear models of pseudo-first order, as depicted in Figure 8 (Mallakpour and Rashidimoghadam, 2019):

$$\ln(q_e - q_t) = \ln q_e - k_1 t \tag{6}$$

$$q_t = q_e(1 - \exp(-k_1 t)) \tag{7}$$

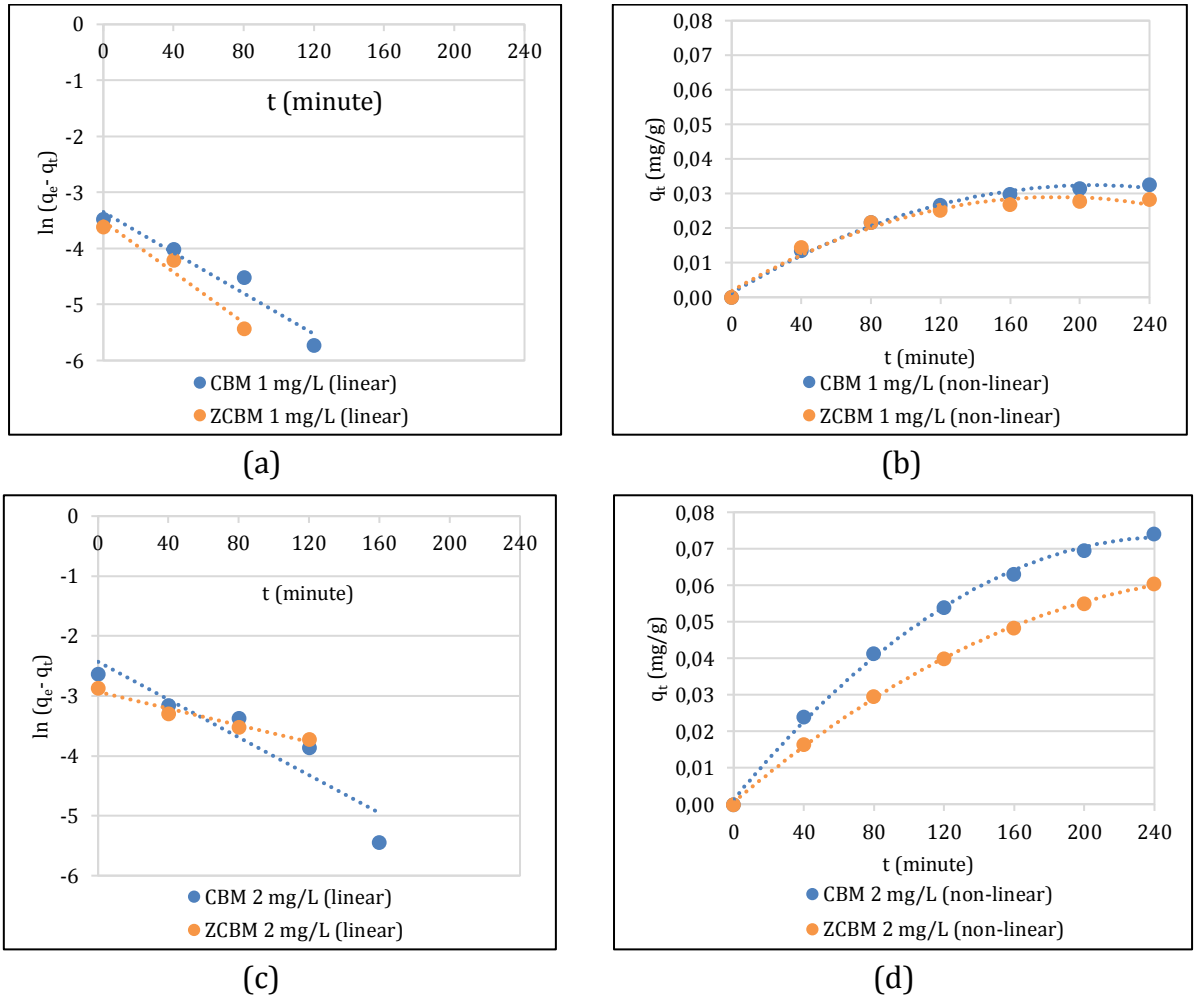

Figure 8 Adsorption kinetics of pseudo first-order at (a) 1 mg/L (*linear*); (b) 1 mg/L (*non-linear*); (c) 2 mg/L (*linear*); and (d) 2 mg/L (*non-linear*) concentrations

A pseudo-second-order kinetic model states that an adsorption rate depends on chemical adsorption, including the electron transfer or sharing between the adsorbate and the adsorbent. Equations 8 and 9 can be used to express the nonlinear and linear models for pseudo-second-order adsorption kinetics, as depicted in Figure 9 (Guo and Wang, 2019):

$$\frac{t}{q_t} = \frac{1}{k_2 q_e^2} + \frac{1}{q_e} t \tag{8}$$

$$q_t = \frac{q_e^2 k_2 t}{1 + q_e k_2 t} \tag{9}$$

The linear method is evaluated based on the compatibility of its equation with the experimental data, whereas a non-linear model is based on these data regression steps. The non-linear method offers a very flexible and fitting curve that reduces the error value (Faghihi, Keykhosravi, and Shahbazi, 2019). To determine the most suitable adsorption kinetics model, it is necessary to compare the regression coefficient (R^2) between linear and non-linear methods. This R^2 value at 1 mg/L and 2 mg/L with the non-linear method ($R^2 >$ 0.97) is higher than that of the linear method. Thus, the non-linear method is more effective for explaining the mercury ion adsorption kinetics model with both adsorbents. Its kinetics are more accurate and stable, and the error distribution is difficult to change (Naushad *et al.*, 2019).

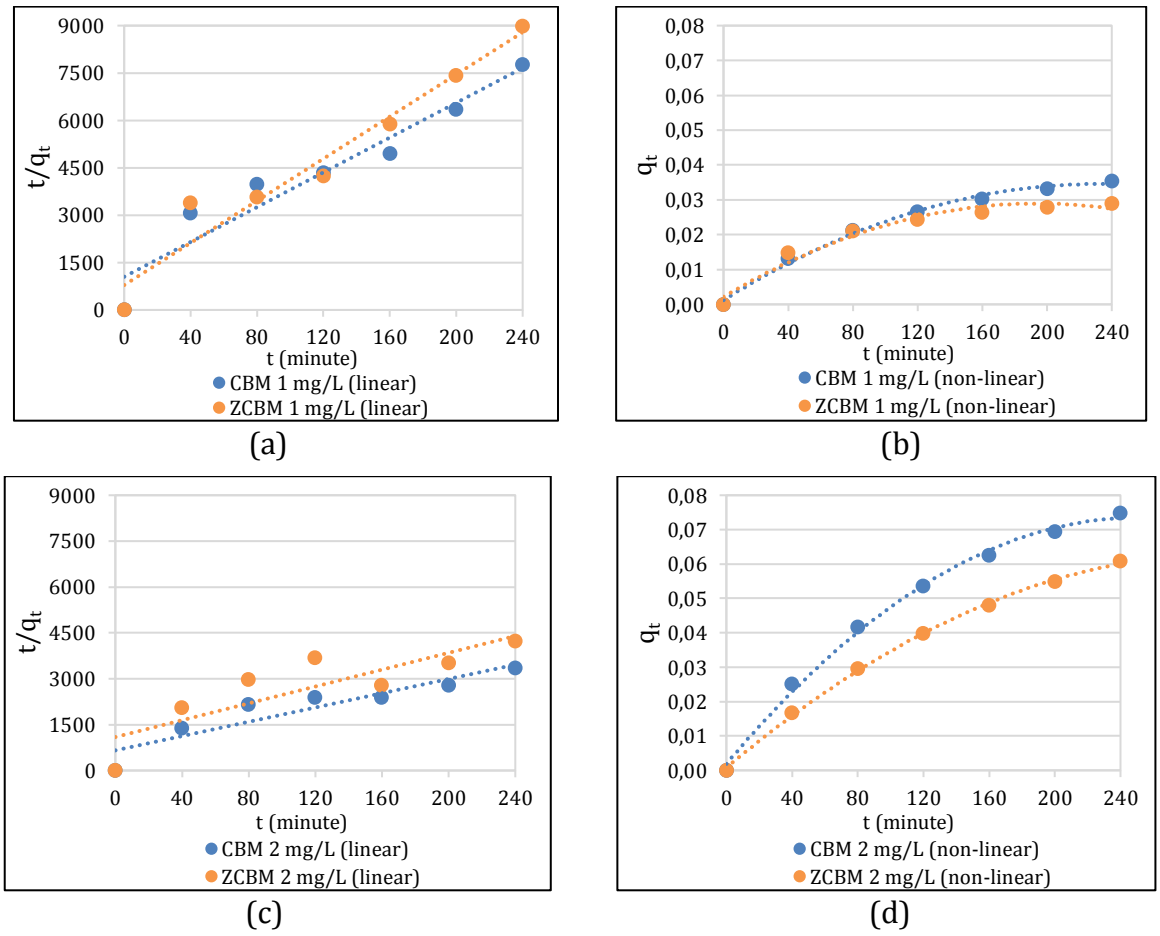

Figure 9 Adsorption kinetics of pseudo second-order at (a) 1 mg/L (*linear*), (b) 1 mg/L (*non-linear*), (c) 2 mg/L (*linear*), and (d) 2 mg/L (*non-linear*) concentrations

Both adsorbents follow the pseudo-first-order kinetics model for adsorption in solutions of 1 mg/L and 2 mg/L with the smallest SSE value. The theoretical adsorption capacity ($q_{e,calcu}$) value resulting from the pseudo-first-order kinetics model is nearer to the value of $q_{e,exp}$ (experimental adsorption capacity). The pseudo-first-order kinetics model indicates that the adsorption rate of adsorbate ions depends on the presence of free active sites in an adsorbent surface. This rate is also directly proportional to the total adsorbate on an adsorbent surface, as proven in the driving force of adsorption (q_e-q_t) that directly depends on the total active sites. The driving force of adsorption gets stronger with the increase in free active sites. The pseudo-first-order model states that the adsorbate ions are bound to a single active site only on the adsorbent surface and that the adsorption takes place physically (physical adsorption). To support the model compatibility, pseudo-first-order kinetics is more effective for an adsorption process in low-concentration solutions, which are 1 and 2 mg/L in the present study. The k_L tends to be lower at a solution concentration of 2 mg/L. According to a theory, the kinetic rate constants of an adsorbate solution are inversely proportional to its initial concentration. The value of the kinetic rate constants decreases as concentration increases because it takes longer for a process or reaction to reach equilibrium at higher concentrations.

4. Conclusions

Characterization by XRD and SEM shows that ZCBM and CBM adsorbents have silica and alumina with high Si/Al ratios and have irregular porous morphology. They have a surface area, average pore diameter, and pore volumes of 36.396 m^2/g, 8.790 nm, 1.800

cm^3/g (ZCBM), and 55.065 m^2/g, 7.812 nm, 2.013 cm^3/g (CBM), respectively. The initial solution concentration affects the mercury adsorption rate. The higher the initial concentration, the stronger the driving force of mass transfer, hence resulting in a significant adsorption rate. The adsorption efficiency tends to rise with the increase in contact time. Based on the two adsorbents investigated, the CBM absorbent had the highest adsorption efficiency (72.3%), followed by ZCBM at 60.8%. Both adsorbents adsorb mercury with the non-linear Langmuir adsorption isotherm model, which has the largest constants of K_L 0.269 L/g and a_L 1.981 L/mg in CBM adsorbents. The maximum monolayer capacity (Qo) is obtained from the ZCBM adsorbent (0.167 mg/g). The adsorption kinetics of mercury for both adsorbents follows a non-linear adsorption kinetics model of pseudo-first-order from the highest R^2 and the lowest SSE values. In line with the findings of this study, CBM has a high potential for removing mercury (II) ions from the water.

Acknowledgments

We would like to express our gratitude for the financial support provided by the Lektor Kepala Research Scheme of Universitas Syiah Kuala's LPPM (with contract No. 74/UN11.2/PP/PNBP/SP3/2019).

References

Ahrouch, M., Gatica, J.M., Draoui, K., Bellido, D., Vidal, H., 2019a. Lead removal from aqueous solution by means of integral natural clays honeycomb monoliths. *Journal of Hazardous Materials*, Volume 365, pp. 519–530

Ahrouch, M., Gatica, J.M., Draoul, K., Vidal, 2019b. Adding value of natural clays as low-cost adsorbent of methylene blue in polluted water through honeycomb monoliths manufacture. *SN Applied Sciences,* Volume 1(1595), pp. 1– 4

Akhtar, F., Anderson, L., Ogunwumi, S., Hedin, N., Bergstrom, L., 2014. Structuring adsorbents and catalysts by processing of porous powders. *Journal of the European Ceramic Society*, Volume 34(7), pp. 1643–1666

Al Hamouz, O.C.S., 2018. New phenol-glycol cross-linked polymers for efficient removal of mercury from aqueous solutions. *Arabian Journal for Science and Engineering,* Volume 43(1), pp. 211–219

Attari, M., 2015. Mercury Removal from Aqueous Solution Using Natural, Synthetic, and Modified Zeolites. *Electronic Thesis and Dissertation Repository*. Available online at https://ir.lib.uwo.ca/cgi/viewcontent.cgi?article=4770&context=etd, Accessed on September 20, 2021

Attari, M., Bukhari, S., Kazemian, H., Rohani, S., 2017. A low-cost adsorbent from coal fly ash for mercury removal from industrial wastewater. *Journal of Environmental Chemical Engineering,* Volume 5(1), pp. 391–399

Bahrudin, N.N., Nawi, M.A., Jawad, A.H., Sabar, S., 2020. Adsorption characteristics and mechanistic study of immobilized chitosan-montmorillonite composite for methyl orange removal. *Journal of Polymers and the Environment*, Volume 28, pp. 1901–1913

Basuki, K.T., Fatuzzahroh, M., Ariyanti, D., Saputra, A., 2021. Adsorption of strontium from an aqueous solution by TiO_2-pillared zeolite. *International Journal of Technology*, Volume 12(3), pp. 625–634

Darmadi, Irfan, M., Iqhramullah, M., Marlina, Lubis, M.R., 2018. Synthesis of chitosan modified polyurethane foam for adsorption of mercury (II) ions. *JBAT*, Volume 7(1), pp. 18–27

Darmadi, Mahidin, Azzahra, S.S., Masrura, M., 2021. Adsorption of mercury (II) ion in aqueous solution by using bentonite-based monolith. In: *Key Engineering Materials*, Trans Tech Publications Ltd, Volume 885, pp. 77–84

Delgado, N., Capparelli, A., Navarro, A., Marino, D., 2019. Pharmaceutical emerging pollutants removal from water using powdered activated carbon: study of kinetics and adsorption equilibrium. *Journal of environmental management*, Volume 236, pp. 301–308

Faghihi, S., Keykhosravi, A., Shahbazi, K., 2019. Modeling of kinetic adsorption of natural surfactants on sandstone minerals: spotlight on accurate prediction and data evaluation. *Colloid and Interface Science Communications*, Volume 33, p.100208

Fang, R.Y., Lu, C.W., Zhang, W.K., Xiao, Z., Chen, H.F., Liang, C., Huang, H., Gan, Y.P., Zhang, J., Xia, Y., 2018. Supercritical CO_2 assisted synthesis of sulphur-modified zeolites as high-efficiency adsorbents for Hg^{2+} removal from water. *New Journal of Chemistry,* Volume 42, pp. 3541–3550

Giraldo, S., Robles, I., Ramirez, A., Florez, E., Acelas, N., 2020. Mercury removal from wastewater using agroindustrial waste adsorbents. *SN Applied Science*, Volume 2(1029), pp. 1–17

Govender, S., Friedrich, H., 2017. Monoliths: a review of the basics, preparation methods and their relevance to oxidation. *Catalysts*, Volume 7(62), pp. 1–29

Guo, X., Wang, J., 2019. A general kinetic model for adsorption: theoretical analysis and modeling. *Journal of Molecular Liquids*, Volume 228, pp. 1–8

Jawad, A.H., Mubarak, N.S.A., Abdulhameed, A.S., 2019a. Tunable Schiff's Base-Cross-Linked Chitosan Composite for the Removal of Reactive Red 120 Dye: Adsorption and Mechanism Study. *International Journal of Biological Macromolecules*, Volume 142, pp. 732–741

Jawad, A.H., Mubarak, N.S.A., Abdulhameed, A.S., 2019b. Hybrid Crosslinked Chitosan-Epichlorohydrin/TiO_2 Nanocomposite for Reactive Red 120 Dye Adsorption: Kinetic, Isotherm, Thermodynamic, and Mechanism Study. *Journal of Polymers and the Environment*, Volume 28, pp. 624–637

Jawad, A.H., Abdulhameed A.S., Abdallah, R., Yaseen, Z.M., 2020a. Zwitterion Composite Chitosan-Epichlorohydrin/Zeolit for Adsorption of Methylene Blue and Reactive Red 120 Dyes. *International Journal of Biological Macromolecules*, Volume 163, pp. 756–765

Jawad, A.H., Abdulhameed, A.S., Mastuli, M.S., 2020b. Mesoporous crosslinked chitosan-activated charcoal composite for the removal of thionine cationic dye: comprehensive adsorption and mechanism study. *Journal of Polymers and the Environment*, Volume 28(3), pp. 1095–1105

Karamah, E.F., Anindita, L., Amelia, D., Kusrini, E., Bismo, S., 2019. Tofu industrial wastewater treatment with ozonation and the adsorption method using natural zeolite. *International Journal of Technology*, Volume 10(8), pp. 1498–1504

Kausar, A., Iqbal, M., Javed, A., Aftab, K., Nazli, Z. i. H., Bhatti, H.N., Nouren, S., 2018. Dyes adsorption using clay and modified clay: a review. *Journal of Molecular Liquids*, Volume 256, pp. 395–407

Khor, S.W., Lee, Y.K., Abas, B.M.R., Tay, K.S., 2017. Application of chalcone-based dithiocarbamate derivative incorporated sol-gel for the removal of Hg (II) ion from water. *ournal of Sol-Gel Science and Technology*, Volume 82(3), pp. 834–845

Lapham, D.P., Lapham, J.L., 2019. Gas adsorption on commercial magnesium stearate: the origin of atypical isotherms and bet transform data. *Powder Tech*, Volume 342, pp. 676–689

Malek, N.N.A., Jawad, A.H., Abdulhameed, A.S., Ismail, K., Hameed, B.H., 2020. New magnetic schiff's base-chitosan-glyoxal/flay ash/Fe_3O_4 biocomposite for the removal of anionic azo dye: an optimized process. *International Journal of Biological Macromolecules*, Volume 146, pp. 530–539

Mallakpour, S., Rashidimoghadam, S., 2019. Poly(vinyl alcohol)/vitamin c-multi walled carbon nanotubes composites and their applications for removal of methylene blue: advanced comparison between linear and nonlinear forms of adsorption isotherms and kinetics models. *Polymer*, Volume 160, pp. 115–125

Mohammed, I.A., Jawad, A.H., Abdulhameed, A.S., Mastulia, M.S., 2020. Physiochemical modification of chitosan with fly ash and tripolyphosphate for removal of reactive red 120 dye: statistical optimization and mechanism study. *Journal of Biological Macromolecules*, Volume 161, 503–513

Nabais, J.V., Carrott, P.J.M., Carrot, M.M.L.R., Belchior, M., Boavida, D., Diall, T., Gulyurtlu, I., 2006. Mercury removal from aqueous solution and flue gas by adsorption on activated carbon fibres. *Applied Surface Science*, Volume 252, pp. 6046–6052

Naushad, M., Alqadami, A.A., Al-Kahtani, A.A., Ahamad, T., Awual, M.R., Tatarchuk, T., 2019. Adsorption of textile dye using para-aminobenzoic acid modified activated carbon: kinetic and equilibrium studies. *Journal of Molecular Liquids*, Volume 296, pp. 1–29

Park, J.H., Wang, J.J., Zhou, B., Mikhael, J.E.R., DeLaune, R.D., 2019. Removing mercury from aqueous solution using sulfurized biochar and associated mechanisms. *Environmental Pollution*, Volume 244, pp. 627–635

Qiu, P., Wang, S., Tian, C., Lin, Z., 2019. Adsorption of low-concentration mercury in water by 3d cyclodextrin/graphene composites: synergistic effect and enhancement mechanism. *Environmental Pollution*, Volume 252, pp. 1133–1141

Rahman, S.K.A., Yusof, N.A., Mohammad, F., Abdullah, A.H., Idris, A., 2017. Ion imprinted polymer monoliths as adsorbent materials for the removal of Hg(II) from real-time aqueous samples. *Current Science*, Volume 113, pp. 2282–2291

Sudibandriyo, M., Putri, F.S., 2020. The effect of various zeolites as an adsorbent for bioethanol purification using a fixed bed adsorption column. *International Journal of Technology*, Volume 11(7), pp. 1300–1308

Ugrina, M., Ceru, T., Nuic, I., Trgo, M., 2020. Comparative study of mercury (ii) removal from aqueous solutions onto natural and iron-modified clinoptilolite rich zeolite. *Processes*, Volume 8(1523), pp. 1–21

Vilela, P.B., Matias, C.A., Dalalibera, A., Becegato, V.A., Paulino, A.T., 2019. Polyacrylic acid-based and chitosan-based hydrogels for adsorption of cadmium: equilibrium isotherm, kinetic and thermodynamic studies. *Journal of Environmental Chemical Engineering*, Volume 7(5), p.103327

Wang, Y.Y., Tang, M.Y., Shen, H., Che, G.B., Qiao, Y., Liu, B., Wang, L., 2018. Recyclable multifunctional magnetic mesoporous silica nanocomposite for ratiometric detection, rapid adsorption and efficient removal of Hg (II). *ACS Sustainable Chemistry & Engineering,* Volume 6(2), pp. 1744–1752

Xu, H., Xie, J., Ma, Y., Qu, Z., Zhao, S., Chen, W., Huang, W., Yan, N., 2015. the cooperation of fesn in a MnO_x complex sorbent used for capturing elemental mercury. *Fuel*, Volume 140, pp. 803–809